Journal of Applied Electrochemistry **30**: 447–455, 2000.

Theoretical analysis of chronoamperometric transients in electrochemical machining and characterization of titanium 6/4 and inconel 718 alloys

A.R. MOUNT[1]*, K.L. ELEY[1] and D. CLIFTON[2]
[1]*Department of Chemistry, and* [2]*Department of Mechanical Engineering, University of Edinburgh, King's Buildings, West Mains Road, Edinburgh EH9 3JJ, Great Britain*
*(*author for correspondence, e-mail: a.mount@ed.ac.uk)*

Received 12 July 1999; accepted in revised form 17 September 1999

Key words: characterization, current analysis, electrochemical machining, inconel 718, titanium 6/4

Abstract

An analytical expression is derived for the current–time transient for electrochemical machining (ECM) using a planar tool and workpiece configuration. This is obtained as a function of such parameters as the initial interelectrode gap, applied voltage, electrolytic conductivity, valency, density and feed rate. Good theoretical fits to experimental data are found for the alloys titanium 6/4 (Ti6/4) and Inconel 718 (In718) using both sodium chloride and sodium nitrate electrolytes, demonstrating the applicability of this theory. The values of the electrolytic molar conductivity obtained for chloride and nitrate are consistent with the expected conductivity obtained from molar conductivity measurements. The mean valency values obtained for Ti6/4 and In718 are 3.5 ± 0.2 and 3.0 ± 0.2, respectively. The fraction of the applied voltage used to drive the electrochemical surface reactions, V_0, has also been obtained. The variation in V_0 between alloys when using the same electrolyte and also for each alloy when using different electrolytes is attributed to differences in the thermodynamics of the removal of the metal from the surface metal oxide. For In718 using chloride electrolyte, an increase in V_0 is observed at higher applied voltages, consistent with a change in the electrochemical dissolution reaction. Analysis of the variation of V_0 at low applied voltages throughout the current–time transient has enabled the current–voltage characteristics of these surfaces electrochemical reactions to be determined, indicating Tafel behaviour. These data show this analysis to be a powerful methodology for understanding and measuring ECM characteristics under realistic ECM conditions.

List of symbols

A	area of electrode (both tool and workpiece)
f	tool feed rate
t	time
z	gap between the electrodes (perpendicular to planar electrode surfaces)
I	current
κ	electrolyte conductivity
ρ	density of the workpiece material
V	applied voltage
V_0	portion of the applied voltage required at the electrode interfaces to drive the machining process
y	thickness of erosion of the workpiece (perpendicular to workpiece surface)
dy/dt	erosion rate
n	valency or number of electrons transferred per dissolving metal atom
F	faradaic constant
M	average molecular mass of the workpiece
I_0	the exchange current for electrochemical reaction
E	potential
b	Tafel slope

Subscripts

∞	value as time approaches infinity
i	initial value (value at time designated as initial time for fitting purposes)
0	value at time zero
1	value at a designated time
2	value at an alternative designated time
C	calculated value

1. Introduction

The conventional milling or turning of high strength, low-weight, metallic and intermetallic alloys can be problematic in cases where the required high cutting forces exceed a tooling capability or are uneconomic because of high tool wear and low machining rates. Electrochemical machining (ECM), a process in which metal is removed by the electrochemical dissolution of a workpiece material, is a technology that has many

potential advantages for the machining of these advanced alloys. Unlike many competing metal shaping processes, ECM is able to machine a material irrespective of hardness and is able to produce complex shapes with high surface integrity at high metal removal rates [1–5]. ECM is carried out by passing an electric current through an electrolyte flowing in the gap between an electrode tool and workpiece. This causes electrochemical dissolution of the workpiece at current densities of the order of 1×10^6 A m^{-2}. As dissolution of the workpiece material occurs the tool electrode is moved, at a controlled rate, to remove material as required. In order to understand, model and control this process, it is important that the physicochemical parameters that control the dissolution are identified. Traditional electrochemical voltammetric [6] measurements have given some insight into the electrochemical dissolution processes occurring at low current densities (below 10^4 A m^{-2}). However, it is extremely unlikely that parameters obtained from these measurements can generally be applied to the high current dissolution region, as the reaction may be affected by the increased voltage and local ion depletion. This means that in the absence of experimental observations, traditional methods for analysing current-voltage data cannot be applied with confidence.

At high currents, parameters which are important in ECM are the electrolyte conductivity (controlled by the concentration and type of ions in the gap between the workpiece and the tool), the valency and the distribution of the applied voltage [7–11]. This is expected to vary with the nature of the workpiece and the current. Previous workers have demonstrated how values of these parameters can be obtained by experimental measurements. For example, Tipton [12] has shown that the 'effective overvoltage' (the portion of the applied voltage used to drive the surface electrochemical reactions) and conductivity can be determined from a plot of the relationship between the applied gap voltage and the gap size when machining at a constant current with no tool feed. The valency is then determined by comparing the mass of material dissolved with the charge passed, assuming constant valency throughout the measurement. However, such simple measurements are a long way from the conditions which are imposed for any practical geometry during electrochemical machining, and in particular where there is a complex interdependence of process parameters over the electrode surface. If such 'static' techniques were to be used, then extensive repeated measurements would be required to check for interparameter sensitivities. To date, there is no analytical method for the dynamic measurement of these parameters during machining [9, 13]. In this paper a novel electrochemical methodology for analysing current–time transients and obtaining these parameters during ECM is reported. The applicability of this method is also demonstrated for Titanium 6/4 (Ti6/4) and Inconel 718 (In718), two commercially important aerospace materials [14, 15].

2. Theory

The system under consideration is a planar tool (cathode) moving at a constant feed rate towards a planar parallel workpiece (anode) of the same area, with electrolyte between the two electrodes (Figure 1). It is assumed that the current is governed by migration (an essential assumption for stable machining). A further assumption is that the electrolyte is being pumped through the interelectrode gap at high enough flow rate that the build-up of machining products and/or the loss of ions from the electrolyte does not significantly affect the electrolyte conductivity, which can be assumed to remain constant throughout the experiment. This is the case for the experimental results presented herein. The current across the electrolyte is given by:

$$I = \frac{\kappa(V - V_0)A}{z} \tag{1}$$

Assuming that this all leads to electrode dissolution, this current is also the dissolution current of the workpiece, and therefore

$$I = \left[\frac{nFA\rho}{M}\right]\frac{\mathrm{d}y}{\mathrm{d}t} \tag{2}$$

The change in the interelectrode distance is given by (Figure 1(a))

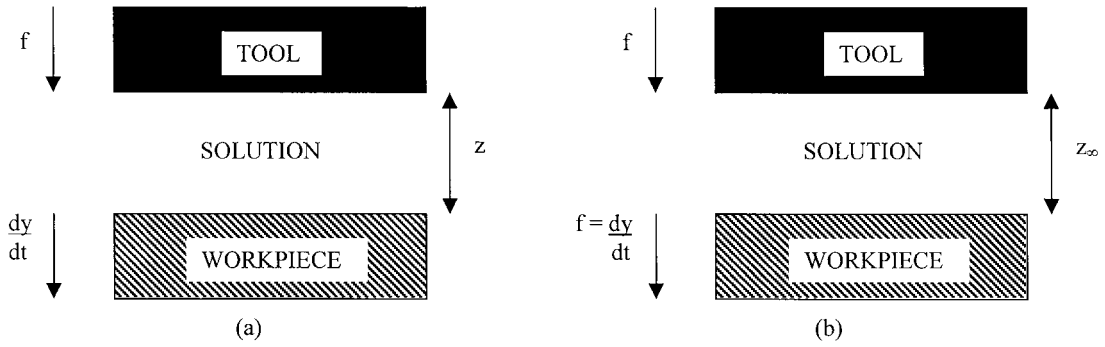

Fig. 1. Schematic representation of the planar tool/planar workpiece configuration (a) before steady-state (b) at steady-state. Relative movement of the tool and workpiece are shown by the arrows, and distance between the electrodes by the double headed arrows.

$$\frac{dz}{dt} = \frac{dy}{dt} - f \tag{3}$$

and hence, combining Equations 1, 2 and 3

$$\frac{dz}{dt} = \frac{k}{z} - f \tag{4}$$

where

$$k = \left[\frac{\kappa(V - V_0)M}{nF\rho}\right] \tag{5}$$

Now at the equilibrium current, I_∞, (I when $t \to \infty$), when a steady-state current has been reached, z remains constant at z_∞ and $dz/dt = 0$ (Figure 1(b)); hence $f = k/z_\infty$ and

$$\frac{dz}{dt} = k\left[\frac{1}{z} - \frac{1}{z_\infty}\right] \tag{6}$$

This equation can be integrated from $t = 0$, $z = z_0$ to $t = t$, $z = z$, to give

$$\ln\left[\frac{z_\infty - z_0}{z_\infty - z}\right] + \frac{z_0 - z}{z_\infty} = \frac{kt}{z_\infty^2} \tag{7}$$

Substituting the appropriate values of I_0, I and I_∞, the currents at $t = 0$, t and ∞ (the equilibrium current time), respectively, from Equation 1 gives

$$\ln\left(\frac{1 - I_\infty/I_0}{1 - I_\infty/I}\right) + (I_\infty/I_0 - I_\infty/I) = \frac{kt}{z_\infty^2} \tag{8}$$

or

$$\ln\left(\frac{1 - I_\infty/I_0}{1 - I_\infty/I}\right) + (I_\infty/I_0 - I_\infty/I) = \frac{f^2 t}{k} \tag{9}$$

Using Equation 9, a series of theoretical curves have been produced for the dimensionless current transients which would be obtained at different values of I_0/I_∞ (corresponding to different values of starting interelectrode distance with respect to the equilibrium machining distance) as a function of dimensionless time, f^2t/k. Figure 2 shows theoretical relationships both when $I_0 < I_\infty$ and when $I_0 > I_\infty$. It is clear that these two sets of transients are very different in shape. When $I_0 > I_\infty$, the dz/dt term dominates the f term in Equation 3 and from Equations 1, 3 and 4, I varies with $t^{-1/2}$ initially, showing a steep decrease in current until the equilibrium current is reached. However, when $I_0 \ll I_\infty$ (the starting interelectrode gap is large), the dissolution current is relatively low and remains so until the feed rate ensures that the gap approaches the equilibrium interelectrode gap, when a sharp rise in current to the equilibrium current is seen, producing S-shaped curves. Although the approach of the current (and gap) is asymptotic to I_∞ (and z_∞), for all practical purposes I reaches the value of I_∞ within experimental error well within the timescale of these plots. For any given value of f, the low dissolution current region becomes more pronounced as I_0 is decreased, since more time is required to reach the equilibrium interelectrode gap.

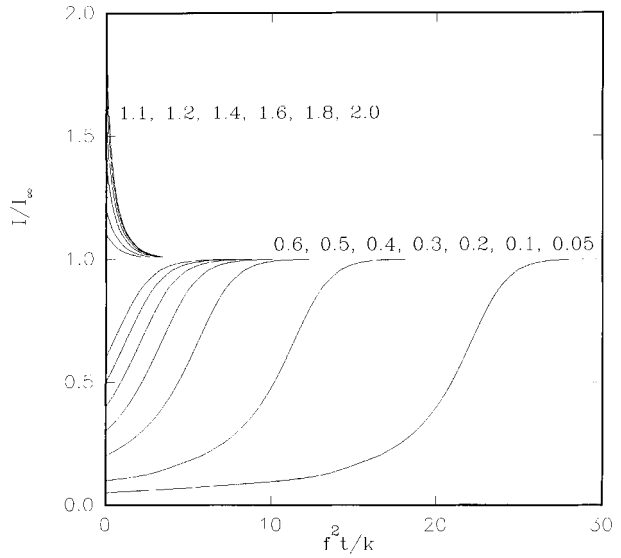

Fig. 2. Theoretical normalised current (I/I_∞) – normalized time (f^2t/k) curves for electrochemical machining using Equation 9. Values of the normalized initial currents (I_0/I_∞) for each series of curves are given on the diagram.

Usually, electrochemical machining experiments involve ensuring that $I_0 < I_\infty$, as this ensures a large starting interelectrode gap and precludes the possibility of shorting or electrolyte breakdown and sparking. Thus, generally rising current transients are observed. However, falling current transients are observed under pulsed voltages, conditions which have recently become of considerable interest [16, 17]. This will be the subject of a future publication. Furthermore, at any given value of I_0, Equation 9 shows that it is k/f^2 which is the characteristic time constant for these transients; thus increasing f or V_0 or decreasing κ or V will decrease the observed transient time for a given system.

3. Experimental details

ECM studies were performed using a Transtec electrochemical machine, (Figure 3). This was combined with a RDOA 100/240/415 regulating transformer (Bonar Brentford Electric) and a 600 A transformer (Goodyear). The solution flow was controlled by means of a Hydriacell D25 pump (Wanner Engineering Inc.); the flow sensor was a type FT 13 (Platon Instrumentation) and the current transducers were of type HT (RS Components). The data were collected using an Intelligent Instruments (Burr–Brown) PC data logging system combined with the Visual Designer software (Intelligent Instruments). The planar cathode (the tool) was a copper–tungsten alloy of length (parallel to the direction of solution flow) 4.00×10^{-2} m and width

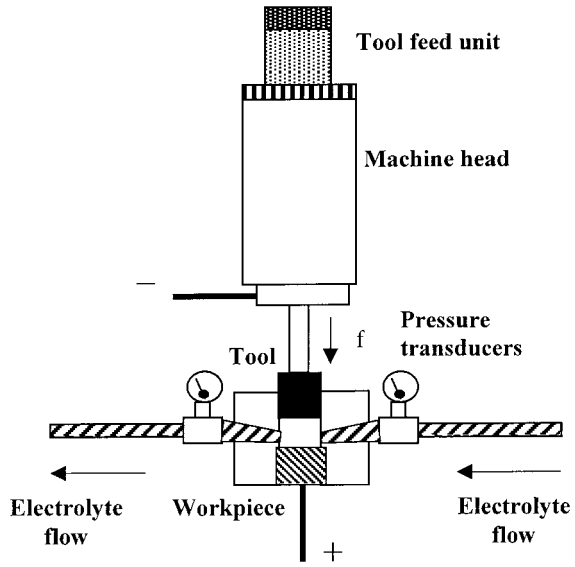

Fig. 3. Schematic diagram of the apparatus used to carry out the electrochemical machining experiments.

(perpendicular to the solution flow) 1.20×10^{-2} m. This gives an area for each electrode of $A = 4.80 \times 10^{-4}\,\mathrm{m}^2$.

The two electrolytes used were 60 litres of 15.0% w/v solution of sodium chloride or of 21.7% w/v solution of sodium nitrate (Anderson, Gibb and Wilson) as appropriate, maintained at 30 °C throughout. These percentage concentrations were chosen to ensure that the ions in solution were of the same molarity (2.56 mol dm^{-3}). The workpiece materials studied were Ti6/4 (Titanium International Ltd) and In718 (Haynes International Inc.). The certified compositions of these alloys were as given in Table 1.

For these data, the initial electrode gap, controlled by inserting a feeler gauge between tool and workpiece, was set at 0.8 mm. The voltage referred to for each experiment is held constant and is the voltage measured between the workpiece and the tool. The electrolyte flow rate and feed rate, f, were maintained at 20 $\mathrm{dm}^3\ \mathrm{min}^{-1}$ and 1.04 mm min^{-1}, respectively. Under these conditions, assuming that one electron results in the consumption or production of one anion or cation in the electrolyte and using this flow rate and an upper limit to I_∞ of 370 A for these experiments, this corresponds to a change in ion concentration of 1.1×10^{-2} mol dm^{-3}. From this the calculated change in electrolyte concentration is 0.4%. These conditions therefore ensure that the assumption of constant electrolyte concentration is applicable, which is confirmed by the observation of a constant equilibrium gap along the flow path for these experiments. Fitting of the current time transients was achieved by iteratively fitting the results to Equation 9, using the SigmaPlot plotting program (Jandel Scientific).

4. Results and discussion

Figures 4 and 5 show representative examples of typical current–time data for Ti6/4 in nitrate electrolyte and chloride electrolyte respectively. Figures 6 and 7 show comparable data for In718. Also shown are the iterative fits obtained using Equation 9. It is clear that good theoretical fits are obtained. To fit these data, a value of I_0/A was obtained from the starting current and the iterative fitting method was used to obtain values of I_∞/A and f^2/k. Values of I_∞/A and f^2/k are reported for these fits in Table 2.

From these and other data it is clear that I_∞/A remains constant at $(59 \pm 3) \times 10^4$ A m^{-2} for Ti6/4 for both types of electrolyte between 10 and 20 V. From Equations 2 and 3 when $\mathrm{d}z/\mathrm{d}t = 0$,

$$\frac{I_\infty}{A} = \frac{nF\rho f}{M} \tag{10}$$

This predicts a constant I_∞/A for any given material, as long as n and f remain constant. It is of course possible that products from the tool and the workpiece reaction could meet in the solution and react, generating species which could return to the electrodes and react further, thereby reducing the efficiency of the machining process. In this case and in contrast to these observations, it is likely that the number of electrons passed in the reaction would change as the workpiece and tool approach each other and good iterative fits to the current–time data would not be expected. Using the measured values of $\rho = 4.413$ g cm^{-3} and the average atomic weight of Ti6/4 (from Table 1), $M = 45.80$ g mol^{-1} in Equation 10 gives a value of $n = 3.5 \pm 0.2$. For In718, the corresponding values are $I_\infty/A = (70 \pm 2) \times 10^4$ A m^{-2}, $\rho = 8.228$ g cm^{-3}, $M = 59.79$ g mol^{-1} and $n = 3.0 \pm 0.2$. These values of n, the average valencies for the alloy, are the important valency parameters for the ECM process.

In principle it is possible to use these values of n to produce values for the valency of each constituent element in these alloys. For example, electrochemical dissolution of Al will be likely to produce Al(III) species, so one possible explanation of these data is that the dissolution of Ti6/4 involves a mixture of Ti(III) and Ti(IV) species, with n for Ti of approximately 3.5 ± 0.2. The observed value for In718 is also consistent with Fe

Table 1. Composition in weight percent of Ti6/4 and In718 alloys

Alloy	C	Fe	N	Al	V	O	Mn	Co	Cr	Cu	Mo	Ni	Si	Ti
Ti6/4	0.01	0.17	0.02	5.89	3.76	0.15	–	–	–	–	–	–	–	89.91
In718	0.05	23.50	–	0.48	–	–	0.22	0.17	18.16	0.02	2.96	53.32	0.10	1.02

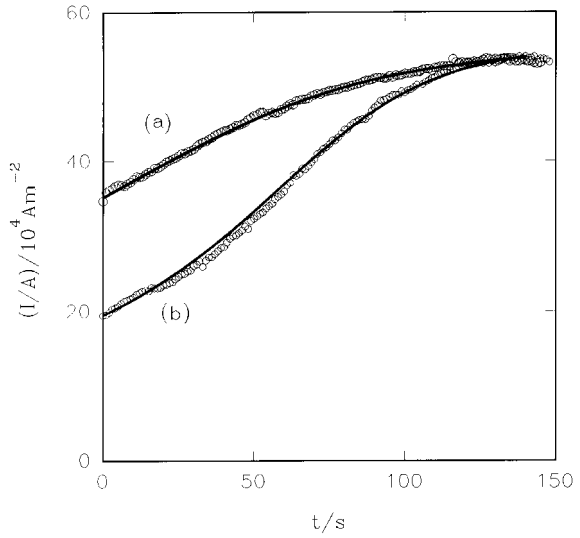

Fig. 4. Typical experimental data (○) for the electrochemical machining of Ti6/4 in nitrate electrolyte at applied voltages, V, of (a) 24 V (b) 18 V. Solid lines show the iterative fits obtained by fitting data to Equation 9.

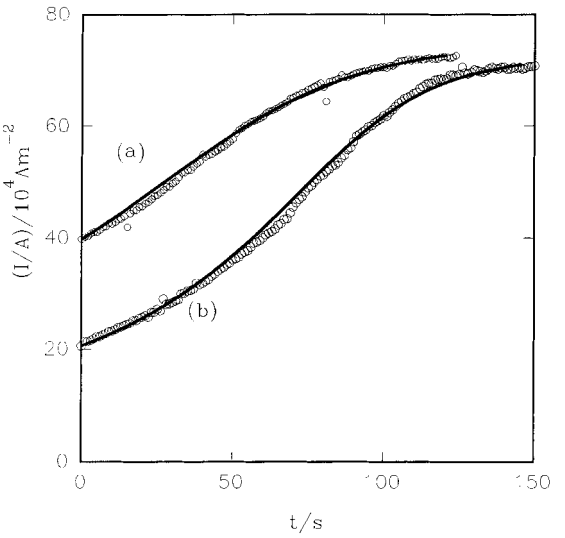

Fig. 6. Typical experimental data for the electrochemical machining of In718 in nitrate electrolyte at (a) 24 V (b) 16 V, plotted in same manner as Figure 4.

dissolving as Fe(III), Cr as Cr(III) and Ni as Ni(III). It is reassuring that these individual elemental valencies are chemically reasonable; however considerable caution must be exercised in assigning individual valencies. For example, previous work on nickel in nitrate electrolyte has suggested that dissolution occurs via Ni(II). Although this observation cannot simply be applied to In718 measurements, as the data were collected at lower current densities and from the pure metal, both of which may cause a change in the elemental valency [18], it is possible that the same mean valency could be achieved by balancing a lower valency for one element (e.g., Ni) with a higher valency for another (e.g., Cr). Thus careful measurements under a variety of elemental compositions close to the alloy composition would be necessary to establish these elemental valencies.

Once these values of n and I_∞ have been obtained from these experiments, it is not necessary to collect the full current time transient, as iterative fitting can be achieved whilst fixing I_∞ at its known value. Thus if I_∞ (or n) is known, values of f^2/k can be obtained experimentally with the consumption of less material or when I_∞ is not attained; for example at relatively small gaps or after the build up of products on recycling of the electrolyte or at lower flow rates, when a passivating surface layer can start to form [19]. However, care must be taken to ensure that the solution flow rate is large enough to ensure that the value of I_∞ is

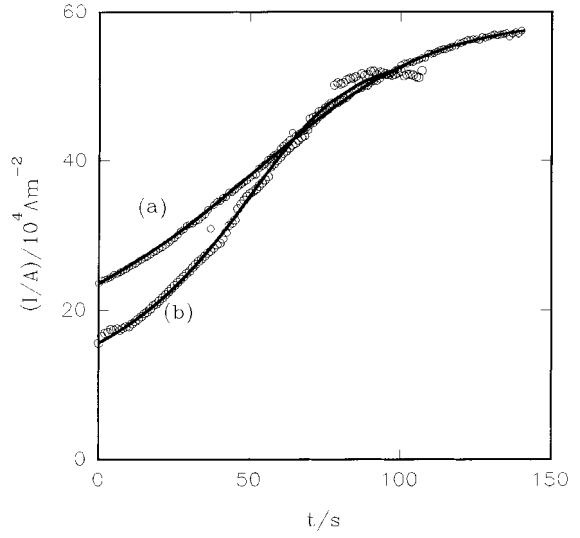

Fig. 5. Typical experimental data for the electrochemical machining of Ti6/4 in chloride electrolyte at (a) 16 V (b) 12 V, plotted in same manner as Figure 4.

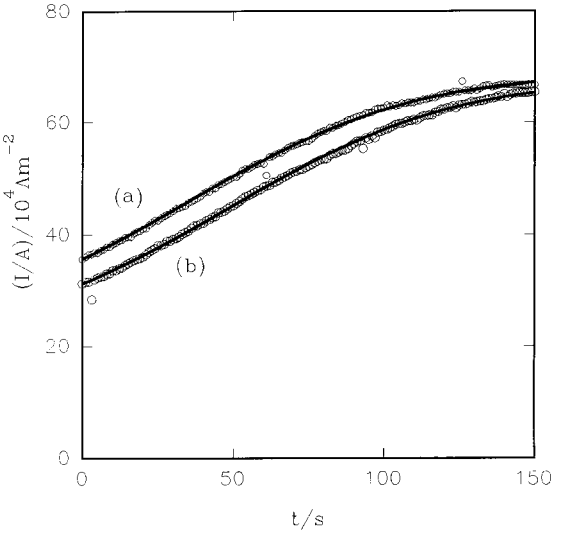

Fig. 7. Typical experimental data for the electrochemical machining of In718 in chloride electrolyte at (a) 24 V (b) 20 V, plotted in same manner as Figure 4.

Table 2. Values of f^2/k and I_∞ obtained from the iterative fits to the experimental current time transients

Electrode	Voltage/V	I_∞/A (/10^4 A m^{-2}) nitrate	f^2/k (/10^{-2} s^{-1}) nitrate	I_∞ /A (/10^4 A m^{-2}) chloride	f^2/k (/10^{-2} s^{-1}) chloride
Ti6/4	10	–	–	57.0 ± 0.1	7.80 ± 0.04
	14	55.7 ± 0.6	7.0 ± 0.1	58.9 ± 0.4	4.83 ± 0.05
	18	55.3 ± 0.1	4.40 ± 0.03	59.5 ± 0.1	3.44 ± 0.03
	20	53.7 ± 0.1	4.34 ± 0.05	61.7 ± 0.1	2.06 ± 0.03
	24	54.2 ± 0.1	3.96 ± 0.04	–	–
In718	12	74.4 ± 0.2	7.36 ± 0.03	71.1 ± 0.6	5.07 ± 0.08
	16	72.4 ± 0.1	5.02 ± 0.02	68.7 ± 0.2	3.41 ± 0.03
	20	70.7 ± 0.1	3.61 ± 0.02	67.9 ± 0.1	3.03 ± 0.01
	24	74.7 ± 0.2	3.51 ± 0.02	69.1 ± 0.1	2.96 ± 0.02

applicable under these conditions. From these iterative fits, the values of f^2/k and I_0/A can be used to determine V_0. From Equation 5,

$$\frac{k}{f^2} = \left[\frac{\kappa(V - V_0)M}{nF\rho f^2}\right] \propto (V - V_0) \tag{11}$$

and, from Equation 1,

$$\frac{I_0}{A} = \frac{\kappa(V - V_0)}{z_0} \propto (V - V_0) \tag{12}$$

since z_0, the starting interelectrode gap is constant in these experiments. Figure 8 shows that for Ti6/4, when k/f^2 and I_0 are plotted against V for these data, straight-line graphs are obtained, consistent with Equations 11 and 12. This indicates that V_0 has a constant value within experimental error under these conditions. In accord with Equations 11 and 12, both the k/f^2 and the I_0 plots show the same V-axis intercept within experimental error. These graphs therefore indicate that $V_0 = 5.4 \pm 0.1$ V and $V_0 = 9.8 \pm 0.5$ V for Ti6/4 in chloride and nitrate electrolyte respectively. Figure 9 shows the corresponding data for In718. As with Ti6/4, both the k/f^2 and I_0 data show a common V-axis intercept, giving values of $V_0 = 5.4 \pm 0.4$ V and $V_0 = 3.0 \pm 0.4$ V for chloride (the low voltage data) and nitrate electrolytes, respectively.

From the gradients of these lines in Figures 8 and 9 and Equations 11 and 12, four independent values for κ for each electrolyte can be obtained. These are all $\kappa = 20 \pm 1$ S m^{-1}, in very good agreement. These values, which have been obtained from the shape of the transients (all t) and the starting current ($t = 0$), respectively, are identical to those measured previously for these electrolyte systems [19]. This good agreement confirms that the products of the electrochemical machining process do not significantly alter the conductivity of the solution as machining progresses, further confirming an assumption of this theoretical treatment.

It is noted that the values of V_0 obtained are lower for chloride than nitrate. This can be explained by the increase in ligating ability when switching from nitrate to chloride. Chloride tends to form relatively strong complexes with the dissolving species at the workpiece

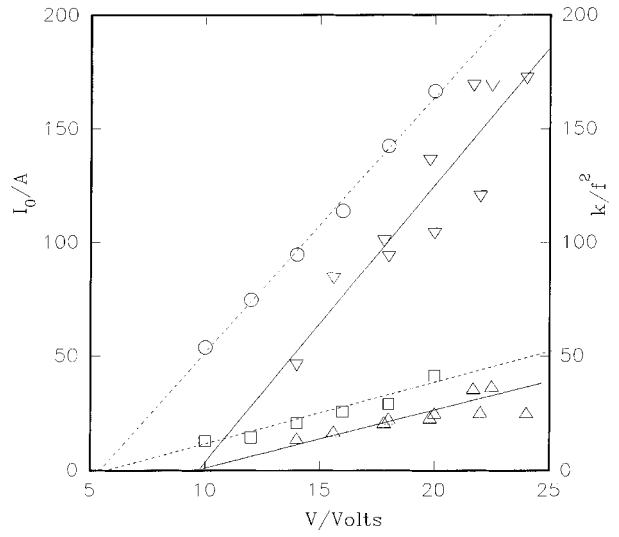

Fig. 8. Plots of I_0 against V for Ti6/4 in (○) chloride (▽) nitrate electrolyte and k/f^2 against V for Ti6/4 in (□) chloride and (△) nitrate electrolyte.

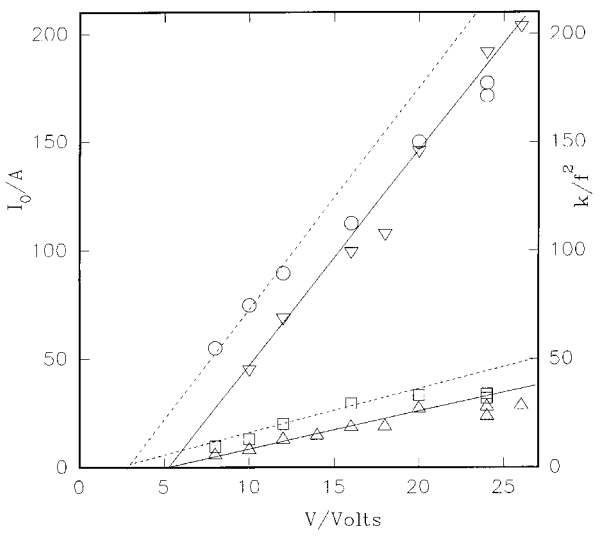

Fig. 9. Plots of I_0 against V for In718 in (○) chloride (▽) nitrate electrolyte and k/f^2 against V for In718 in (□) chloride and (△) nitrate electrolyte.

and this would lead to a decrease in the free energy of the dissolution process and hence a decrease in the oxidation potential. Also, V_0 varies with the nature of the alloy. There are potentially two different types of surface process occurring. If the reaction were simply the oxidation and dissolution of the metals as ions from the metal surface, then the observed values of V_0 would be expected to be less for Ti6/4 than In718, as the oxidation of both Titanium and Aluminium metal are thermodynamically favoured over Iron, Chromium and Nickel [20]. In fact V_0 for In718 is consistently lower than V_0 for Ti6/4, which indicates that the dissolution reaction involves the expulsion of the metal ions from the surface oxide, as the free energies of formation of titanium and aluminium oxides are much higher than those of iron, nickel and chromium oxides [21, 22]. This will lead to an increase in the energy required to expel metal ions from the Ti6/4 oxide with respect to In718 and hence to an increase in the value of V_0.

At higher applied voltages (16 V and above) for In718 in chloride both the k/f^2 and the I_0 data show systematic deviation from this line. This is consistent with an increase in the value of V_0 at these voltages, so that V_0 approaches the value observed for nitrate. Two possible explanations for this effect are also a decrease in the electrolyte conductivity and an increase in the resistance of an insulating surface layer on the workpiece. However, these can be rejected since a decrease in conductivity would cause an increase in the equilibrium gap and significant resistive *IR* drop due to a surface film would cause a current dependent deviation in the value of V_0 and result in a poor iterative fit to the current–time data. Neither of these effects is observed.

The most likely explanation is a change in the surface dissolution reaction mechanism, which would correspond to a plateau in the anodic current–voltage curve for this electrode. Similar behaviour has been previously observed for nickel in nitrate electrolyte [23], and was attributed to a change in nature of the surface oxide film inducing a change in the reaction. This is at present the subject of further investigation.

The apparent insensitivity of the observed values of V_0 with current is worthy of discussion. V_0 corresponds to that part of the applied voltage at the electrode surfaces, driving the electrochemical reactions. It is extremely difficult to produce a general theory for the quantitative analysis of I, V_0 characteristics, but the reactions that need to be considered are

$$M(s) \rightarrow M^{n+} + ne^-$$

at the workpiece (where M is the metal and n is its valency) and

$$H_2O + e^- \rightarrow \frac{1}{2}H_2(g) + OH^-(aq)$$

at the tool. At each electrode, the experiment is carried out under conditions of efficient mass transport, and at high currents, where the back reactions can be neglected. In this case Tafel behaviour should be observed. This is supported by the few experimental measurements which have been performed on different materials under similar conditions [24, 25]. In this case, the following general equation should apply

$$V_{0.2} - V_{0.1} = b \ln(I_2/I_1) \quad (13)$$

where b is the Tafel slope. Thus, at first sight, from Equation 13, V_0 would be expected to be dependent on current rather than independent of current as is found in the experimental data. The observed independence indicates that the change in V_0 with I is small and within experimental error for these data. In this case, the effect would only seen at applied voltages, V, sufficient to enable machining but sufficiently small that significant changes in $(V - V_0)$ occur during the time course of the current transient. This can be seen in the data collected at the lowest applied voltages, as shown in Figures 10(a) and 11(a), where calculated values of time, t_C, obtained by using the parameters from the iterative fit of the experimental data to Equation 9 are plotted against the experimental values of time, t, for two applied voltages, 11 and 12 V respectively. The data in Figure 10(a) show a systematic deviation of this line from a line of unity gradient and zero intercept at higher values of t, which is consistent with an increase in V_0 with increasing current. A similar deviation is also observed in Figure 11(a), although this is not as marked, due to the decrease in the relative change in $(V - V_0)$ brought about by the increase in V. This plot demon-

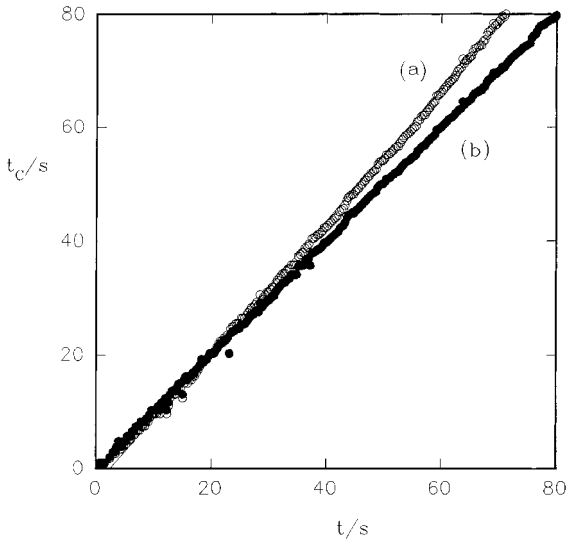

Fig. 10. Plots of t_C (calculated time) against t (experimental time) for electrochemical machining of In718 at an applied voltage of $V = 11$ V in nitrate electrolyte. (a) Iterative fit to the whole data set using Equation 9, with t_C being calculated from the resulting parameters and the observed current values. Equation of straight line is $t_C = 1.158\,t - 2.854$; correlation coefficient, $r = 0.9927$. (b) Fits to Equation 17 using successive iterative fits to 9 s portions of the data, followed by calculation of t_C values as in (a). Equation of straight line is $t_C = 1.004\,t - 0.198$; correlation coefficient, $r = 0.9998$.

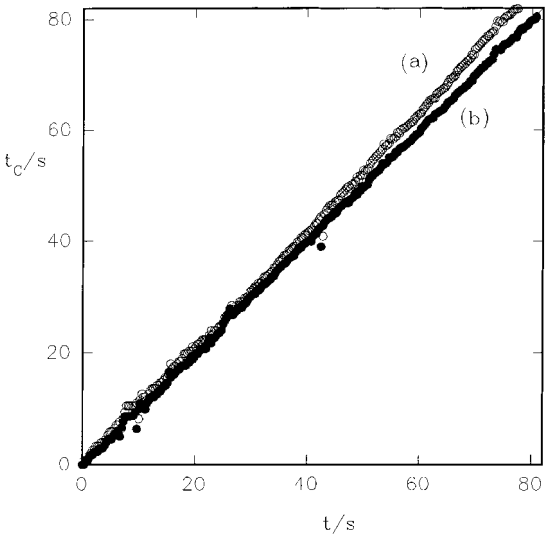

Fig. 11. Plots of t_C (the calculated time) against t (the experimental time) for electrochemical machining of In718 at an applied voltage of $V = 12$ V in nitrate electrolyte. (a) Iterative fit to the whole data set using Equation 9, with t_C being calculated from the resulting parameters and the observed current values. Equation of straight line is $t_C = 1.058\,t - 0.166$; correlation coefficient, $r = 0.9996$. (b) Fits to Equation 17 using successive iterative fits to 9 s portions of the data, followed by calculation of t_C values as in (a). Equation of straight line is $t_C = 1.003\,t - 0.241$; correlation coefficient, $r = 0.9998$.

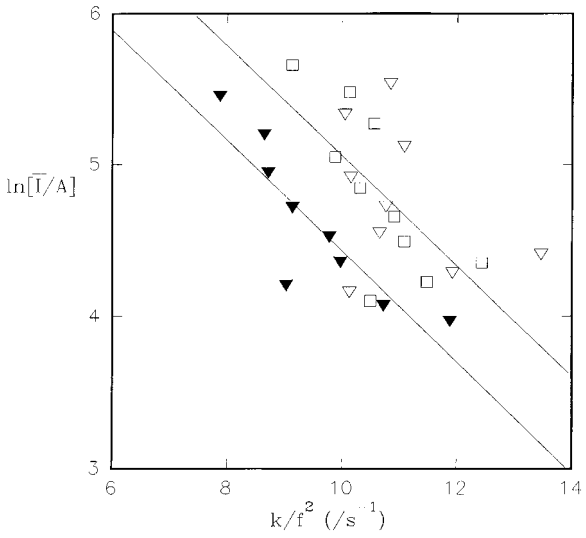

Fig. 12. Plot of $\ln(\bar{I})$, the logarithm of the mean current for each 9 s portion against the corresponding value of k/f^2 obtained from the iterative fits in Figures 10(b) and 11(b) for In718 in nitrate electrolyte at an applied voltage, $V = 11$ V (solid points), $V = 12$ V (open points). Straight line through the 11 V data is the regression line. Line through the 12 V data is that expected from Figure 9 if the same $\bar{I}$, V_0 behaviour were observed in each case.

strates why the iterative fits presented previously show a reasonable fit to the data, as when the voltage, V, applied to the system is increased above 12 V the change in the magnitude of $(V - V_0)$ throughout the transient becomes sufficiently small that the approximation of a constant value of $(V - V_0)$ is applicable.

For the 11 and 12 V data, it is possible to determine how V_0 varies throughout the transient. In this case, Equation 6 can be integrated from $t = t_i$, $I = I_i$ to $t = \infty$, $I = I_\infty$ to give

$$\ln\left(\frac{z_\infty - z_i}{z_\infty - z}\right) + \frac{z_i - z}{z_\infty} = \frac{k(t - t_i)}{z_\infty^2} \tag{14}$$

and hence,

$$\ln\left(\frac{1 - I_\infty/I_i}{1 - I_\infty/I}\right) + (I_\infty/I_i - I_\infty/I) = \frac{f^2(t - t_i)}{k} \tag{15}$$

where $t > t_i$ and the equation is referenced to an initial measurement of t_i, I_i. Since I_∞ is known from previous measurements at higher applied voltages, this equation can be applied over a range of $(t - t_i)$ values, as long as the change in I is sufficiently small to ensure that V_0 (and hence f^2/k) can be assumed to be constant. Iterative fits of the data to Equation 17 have been obtained at various values of t_i, with $(t - t_i) \leqslant 9$ s. This ensures that V_0 is constant, as the variation in I is 5% or less of I_∞. Figures 10(b) and 11(b) show the resulting values of t_C, which show the fits to be much improved compared with Figures 10(a) and 11(a).

Using these fits, a graph of the variation of k/f^2 with $\bar{I}$, the mean current of the section of data used for each fit, can be plotted, as shown in Figure 12. From Equation 11, the variation in k/f^2 in this case is due to changes in $-V_0$ and a graph of $\ln(\bar{I})$ against k/f^2 should be a straight line with a negative gradient if Tafel behaviour is observed. This is indeed the case. From the gradient of the k/f^2 plot in Figure 9 and since this variation in I with V_0 should be independent of the applied voltage (assuming no change in reaction mechanism) the equivalent data for an applied voltage of 12 V should fall on a parallel line, displaced by 2.0 s^{-1} on the k/f^2 axis. Despite the increased scatter, consistent with the increase in the error associated with measuring these data as V becomes the dominant term in $(V - V_0)$, there is reasonable agreement between these data and this line, which confirms Tafel behaviour (Equation 13). These lines each produce a value of $b \approx 1.4$ V.

This method of analysing portions of the current–time transient applies not only where there are changes in $(V - V_0)$, but also when there are changes to any of the constituent parameters of k. Thus changes in κ, due to the formation of bubbles, or to changes in the nature and concentration of ions in the gap can be measured by systematic variation of electrolyte flow rate in the latter case, and the inlet and outlet pressure of the electrolyte flow in the former, even in situations where an equilibrium machining current is not achieved.

5. Conclusions

The results presented in this paper clearly demonstrate that analysis of chronoamperometric electrochemical

machining data using a planar tool/planar workpiece geometry can be used to characterise the dissolution process of Ti6/4 and In718 under conditions (current density, flow velocity, voltage and feed rate) applicable to machining. In these cases, dissolution occurs with little significant resistance from surface layers, and values can be obtained which allow the voltage required to initiate significant machining to be obtained and the nature of the dissolution process to be probed, as well as the conductivity of the electrolyte and the valency of the reaction to be measured. Furthermore, current–voltage characteristics of the surface electrochemical reactions can be also obtained under conditions relevant to ECM.

It is clear that this approach has wide applicability in the study of electrochemical machining as it allows dynamic parameterization of the machining process and thereby gives insight into the electrochemistry of the dissolution process. Furthermore, it should also be invaluable in probing changes in such variables as electrolyte conductivity and V_0 (from fits to the shape of the curve) and valency (from changes in the value of I_∞ during machining) under conditions where these effects are important. Finally, this treatment can be extended to the analysis of the current–time transients of multiple electrodes which can be used to probe the spatial variation of these effects. This approach is being exploited in extending our studies of electrochemical machining to other alloys.

Acknowledgement

We wish to thank the Materials Initiative, Faculty of Science, University of Edinburgh for the summer studentship for KLE on which much of this work was done.

References

1. D.G. Risco and A.D. Davydov, *J. Am. Soc. Mech. Eng.* **64** (1993) 701.
2. M.A. El Dardery, *Int. J. Machine Tool Design Res.* **22**(3) (1982) 147.
3. B. Kellock, *J. Machinery and Product. Eng.* **140**(3604) (1982) 40.
4. O.V.K. Chetty and R.V. Murthy Radhakrishan, *Trans. ASME J. Eng. Ind.* **103**(3) (1981) 341.
5. A.R. Mileham, S.J. Harvey and K.J. Stout, *J. Wear* **109** (1986) 207.
6. M. Datta, *J. Res. Dev.* **37**(2) (1993) 207.
7. A.K. Karimov, *J. Sov. Aeronautics* **28**(3) (1985) 105.
8. A.G. Makie, *J. Math. Anal. Appl.* **117**(2) (1986) 548.
9. J. Kozak, L. Dabrowski, K. Lubkowski and M. Rozenek. Proceedings of the 13th International CAPE Conference, Warsaw (1997), p. 311.
10. H. Tipton, Proceedings of the 5th International Confererence on 'Advances in Machine Tool Design and Research' (1964) p. 509.
11. A.D. Davydov and V.D. Kanshcheev, *Elektronnaya Obrabotka Materialov* (1985) 80.
12. H. Tipton, *Machine. & Prod. Eng.* (1968) 325.
13. V.K. Jain and K.P. Rajurkar, *Precision Eng.* **13**(2) (1991) 111.
14. M. Atkey, *Indust. Robot* **12**(4) (1985) 231.
15. D.J. Jones, *Chem. Brit.* (1988) 1135.
16. B. Wei and J. Kozak, *Trans. NAMRI/SME* **22** (1994) 147.
17. M. Datta and D. Landolt, *Electrochim. Acta.* **26**(7) (1981) 899.
18. A.D. Davydov, E.N. Kiryak, A.N. Ryabova, V.D. Kashcheev, B.N. Kabanov, *Elektronnaya Obrabotka Materialov* **5** (1979) 19.
19. C.N. Larsson, *in* 'Electrochemical. Machining' edited by A.E. De Barr, D.A. Oliver (MacDonald, London, 1968), p. 108.
20. 'CRC Handbook of Chemistry and Physics', 74th edn, edited by D.R. Lide (CRC Press, Florida, USA, 1993).
21. R.D. Harrison (Ed.), 'Book of Data', Nuffield Advanced Science. (Penguin Books, Harmondsworth, UK, 1972).
22. F.J. DiSalvo and S.J. Clarke, *Current Opinion Solid State & Mater. Sci.* **1** (1996) 241.
23. M. Datta and D. Landolt, *J. Electrochem. Soc.* **122** (1975) 1466.
24. D. Landolt, R.H. Muller, C.W. Tobias, *J. Electrochem. Soc.* **118** (1971) 40.
25. J. Hives and I. Rousar, *J. Appl. Electrochem.* **23** (1993) 1263.